Geophys. J. Int. (1999) **136,** 519–536

A global isostatic gravity model of the Earth

Mikhail K. Kaban,[1] Peter Schwintzer[2] and Sergey A. Tikhotsky[1]

[1] *Institute of Physics of the Earth, Russian Academy of Sciences, Moscow, Russia*

[2] *GeoForschungsZentrum Potsdam, Div.* 1 *'Kinematics and Dynamics of the Earth', Germany. E-mail: psch@gfz-potsdam.de*

Accepted 1998 September 14. Received 1998 July 13; in original form 1997 May 13

SUMMARY

The long-wavelength features of the external gravity field of the Earth contain the gravitational signal from deep-seated lateral mass and density inhomogeneities sustained by dynamic Earth mantle processes. To interpret the observed gravity field with respect to mantle dynamics and structures, it is essential first to remove the lithosphere-induced anomalous gravitational potential, which is generated by the topographic surface load and its isostatically compensating masses. Based upon the most recent global compilation of crustal thickness and density data and the age distribution of cooling oceanic lithosphere, residual topography and gravity are calculated by subtracting the 'known' crustal and oceanic lithosphere compensating masses and gravitational e ects from the surface fields. Empirical admittances between residual topography and gravity are then computed to estimate the e ective depths of the remaining compensating masses, which are not explained by the initial data and model assumptions. This additional compensation is eventually placed by adjusting the density in the uppermost mantle between the Moho and, on average, 70 km depth, with a maximum of 118 km under Tibet. The lithospheric mass distribution is used in a subsequent forward computation to create a global model of the lithosphere-induced gravitational potential. The resulting isostatic model is considered to be valid for spatial wavelengths longer than 500 km. The isostatic lithosphere model field, expressed in terms of both gravity and geoid heights, is subtracted from the observed free-air gravity field to yield a global set of $1^\circ \times 1^\circ$ isostatic gravity disturbances and from a satellite-derived long-wavelength geoid to yield the isostatic residual geoid. The comparison of residual (mantle) gravity, residual topography and isostatic corrected gravity allows us to identify the main characteristics of the underlying mantle; for example, dynamic support by mantle flow of the North Atlantic topographic high. Applying the isostatic correction, the overall pattern of the geoid becomes smoother and the most pronounced features, which are separated in the observed geoid, tend to get connected to larger structures. These results stress the importance of separation of the lithospheric gravitational impact for a correct interpretation of the external gravity field, even in its very long-wavelength constituents. Also, the isostatic corrected geoid spectrum reveals a stronger decrease in power from degree 3 to degree 4 and degree 5 to degree 6, which is in accordance with seismological models of deep-mantle structures.

Key words: geoid, gravity, isostasy, lithosphere.

1 INTRODUCTION

The gravity field at the Earth's surface is recovered in its long-wavelength constituents from the analysis of observed satellite orbit perturbations and in its medium- to short-wavelength features from the evaluation of satellite altimeter data over the oceans and observed gravity anomalies over the continents. State-of-the-art global gravity field models represent the long-wavelength geoid down to spatial wavelengths of about 1500 km with a homogeneous accuracy of about 50 cm, decreasing to about 100 cm for a spatial resolution of 500 km with increasing accuracy di erences between oceanic, continental and polar areas due to the available observation data. In terms of gravity, the model errors accumulate to a value of 3 mgal, on average, at a resolution of 500 km. Although these accuracy figures have to be improved for detailed studies, the signal-to-noise

ratios are large enough for quantitative investigations on the general density and mass distribution of the Earth's lithosphere and deeper interior.

A knowledge of the distribution of density inhomogeneities in the Earth's interior is essential for modelling geodynamic processes. The external gravity field and geoid as observed at the surface of the Earth contain information on the density and mass distributions, thus their use for a reconstruction of deep Earth structure and dynamics seems to be adequate. However, gravity variations and geoid undulations reflect the influence of density inhomogeneities at every point integrated over the whole Earth, making a unique inversion impossible.

To study a particular layer of the Earth's interior from a gravity field's point of view, the gravitational e ects of the remaining part have to be reduced by appropriate model assumptions. Thus, when studying the deep-seated inhomogeneities of the Earth's mantle by gravity field analysis, the e ects of the structure of the lithosphere have to be taken into consideration. It is generally accepted that deep structures or mantle flows mainly show up in the long-wave components of the gravity field and geoid. Thus, averaged free-air anomalies and low harmonic geoid undulations are often used for Earth mantle studies. Investigations have shown, however, that the mass distribution within the lithosphere also significantly a ects the long-wave features of the global geoid (Chase & McNutt 1982; Dahlen 1981; Hager 1983; Le Stun & Ricard 1995; Lister 1982). The same e ect was analysed in terms of gravity anomalies by Artemjev *et al.* (1994).

An attempt to remove the lithosphere e ect from the observed global geoid was made in some of the papers cited above using isostatic modelling to account for topography and compensating masses. The calculations either adopt idealized isostatic models for the whole Earth or use topography and seismic data on the crustal structure and/or try to adjust one or a few general parameters relating to crustal lithosphere thickness and density variations. Over the oceans the model of the cooling oceanic lithosphere is applied to compute the thermal state and density of oceanic lithosphere, which are dependent on its age inferred from crustal magnetization (e.g. Cazenave 1986). In this study, the lithospheric structure is estimated based upon the most recent global compilation of crustal data (Mooney *et al.* 1998) augmented by higher-resolution data in certain regions. Over the oceans, the cooling oceanic lithosphere concept based upon the digital ocean-floor age grid (Müller *et al.* 1993) is applied. After a subtraction of the 'known' compensating masses, the residual topography and gravity are analysed by admittance calculations to introduce geology-dependent subcrustal density variations for a complete mass balance in the Earth's upper layers. One of the principal goals of the present study is to investigate how the characteristics of and variations in lithospheric isostatic compensation a ect the isostatic residual geoid and gravity, both on a global basis and restricted to long-wavelength features.

This means the construction of a consistent model of isostatic corrections in terms of both gravitational accelerations and geoid undulations. Applying the isostatic model to the observed external gravity field and the geoid results in an isostatic gravity field and an isostatic residual geoid, which are free from the gravitational e ects of topography and compensating masses. A comparison of residual gravity, residual topography and isostatic corrected gravitational potential then gives some idea of the geophysical sources of the surface signals, for example either static mass compensation in the upper mantle or dynamic support by mantle flow of excess topographic loading, or a mixture of both.

To emphasize the importance of subtracting the e ect of the lithosphere from the observed gravity and geoid when looking for dynamic mantle processes, a comparison in terms of a statistical analysis of the derived isostatic residual geoid with general features of mantle heterogeneities inferred from seismological data is made to reveal common features in the power spectra that are not visible in the observed geoid.

2 INITIAL DATA

2.1 Gravity and topography data

To obtain a global coverage of high-resolution gravity information, the EGM96 spherical harmonic expansion of the gravitational geopotential up to degree and order 360 (Lemoine *et al.* 1998) was used to derive mean gravity block values related to an $1^\circ \times 1^\circ$ equal-angle grid. EGM96 is a gravity field model incorporating satellite tracking data, GEOSAT and ERS-1 altimeter data, and the most up-to-date global compilation of gravity data, including recently released data sets over e.g. Greenland, China and the former Soviet Union.

For geophysical modelling on a global scale, it is reasonable to work in terms of gravity disturbances rather than gravity anomalies (Chapman & Bodine 1979). Both terms are defined as the di erence between actual gravity at a point P of the geoid and normal gravity, generated by a conventional ellipsoid of revolution. Whereas for gravity anomalies normal gravity is taken at a point Q projected to the surface of the ellipsoid, for gravity disturbances normal gravity is computed at the same point P. Consequently, the di erence between a free-air gravity anomaly Δg_{FAA} and a free-air gravity disturbance δg_{FAA} is given by the vertical normal gravity gradient multiplied by the geoid height N (Heiskanen & Moritz 1967),

$$\delta g_{\mathrm{FAA}} = \Delta g_{\mathrm{FAA}} - \frac{\partial \gamma}{\partial h} N . \qquad (1)$$

With $\partial\gamma/\partial h \approx -0.31$ mgal m^{-1}, the di erence between free-air gravity disturbances and anomalies will be up to ± 30 mgal, increasing the amplitudes of the main features when switching from gravity anomalies to disturbances due to the in general positive correlation between long-wavelength gravity and geoid height variations.

The mean $1^\circ \times 1^\circ$ gravity disturbances are computed from the EGM96 gravitational coe cients after having subtracted the normal gravitational even-degree zonal terms of a chosen conventional reference ellipsoid. Throughout this paper the GRS67 (IAG 1971) reference system is used.

The geographical distribution of the EGM96 gravity disturbances is shown in Fig. 6(a). The weighted root mean square of the $1^\circ \times 1^\circ$ block values amounts to 25.2 mgal with a weight equal to the cosine of the block's latitude attributed to each value. The values range from -304 to 344 mgal. The accuracy of the gravity information underlying the EGM96 model solution is estimated to be about 5 mgal on average (maximum 60 mgal) for terrestrial gravity, and 2 mgal (maximum 25 mgal) for altimeter-derived gravity anomalies (Kenyon & Pavlis 1996).

Earth surface topography, again related to a $1^\circ \times 1^\circ$ equal-angle global grid, was taken from the OSU90 $1^\circ \times 1^\circ$ gravity and topography data set (Rapp & Yi 1991), which includes

elevation and bathymetric data based on the TUG87 30′ elevation file (Wieser 1987). Over the area of the former Soviet Union, the OSU elevation data were replaced by a more recent compilation made by Artemjev *et al.* (1994).

2.2 Global geoid

The most homogeneous global representation of the long-wavelength geoid is taken from an actual satellite-only global gravity field model. The GRIM4-S4 model (Schwintzer *et al.* 1997) is a joint German/French gravity field solution deduced through orbit perturbation analysis techniques from optical, laser and microwave tracking data of 34 satellites. The model is a solution in spherical harmonics with a computational spectral resolution of the gravitational coe cients up to degree and order 60, obtained in a rigorous least-squares adjustment. The degree one terms are fixed to zero; that is, the model is referred to the Earth's centre of mass. Due to the attenuation of the gravitational signal with the satellites' orbit altitude, the resolution of the GRIM4-S4 model can be considered to be complete up to about degree and order 30, which is su cient for the purpose of this study, where only the very long-wavelength part of the gravitational spectrum is of importance.

From the given GRIM4-S4 gravitational coe cients, the geoid heights are computed, again referred to the GRS67 reference ellipsoid and normal potential. The signal and error degree variances of the GRIM4-S4 geoid, and the geographic distribution of the geoid undulations' standard deviations estimated by a rigorous error propagation are given in Fig. 1. Fig. 7(a) depicts the GRIM4-S4 geoid, taking into account all terms up to degree and order 30. The commissioning error up to degree and order 30 accumulates to a value of 60 cm for a computed geoid undulation, on average. The degree variance (spectral power) for degree one is defined by

$$\sigma_l^2 = \sum_{m=0}^{l} (c_{l,m}^2 + s_{l,m}^2), \qquad (2)$$

where $c_{l,m} = \Delta\bar{C}_{l,m}$, $s_{l,m} = \bar{S}_{l,m}$, if expressed in terms of non-dimensional harmonic geopotential coe cients, and $c_{l,m} = R\Delta\bar{C}_{l,m}$, $s_{l,m} = R\bar{S}_{l,m}$, if expressed in terms of geoid heights, where l, m are the degree and order of the spherical harmonic coe cient, $\Delta\bar{C}_{l,m}$, $\bar{S}_{l,m}$ are the fully normalized spherical harmonic coe cients with respect to the normal potential of a reference ellipsoid, and R is the equatorial radius of the Earth. To compute error degree variances the coe cients $\bar{C}_{l,m}$, $\bar{S}_{l,m}$ are replaced by their estimated standard deviations $s(\bar{C}_{l,m})$, $s(\bar{S}_{l,m})$.

2.3 Thickness and density of the main crustal layers and age of the oceanic lithosphere

To estimate the anomalous gravity of the crust, crustal parameters (thickness and density of sediments and consolidated crust layers) taken from the most up-to-date $5^\circ \times 5^\circ$ global crustal model CRUST 5.1 (Mooney *et al.* 1998) supplemented by some regional data sets were used. The initial $5^\circ \times 5^\circ$ values were interpolated onto the same $1^\circ \times 1^\circ$ grid as used for the initial gravity and topography data sets. For central and northern Eurasia the CRUST 5.1 values were replaced by the original $1^\circ \times 1^\circ$ data from Artemjev *et al.* (1994), which are more detailed in describing the thickness and density of sediments and the Moho depth. Crustal thickness in western Europe was corrected using the $1^\circ \times 1^\circ$ map published in the Geothermal Atlas of Europe (Hurtig *et al.* 1992); the same was done for North America using the map from Mooney & Braile (1989). Ice-sheet thickness information was taken from the $1^\circ \times 1^\circ$ original maps of Drewry (1983) for Antarctica and Mooney *et al.* (1998) for Greenland. For all ocean regions, regardless of their ocean-floor age, a 7.2 km thick consolidated crust was initially assumed (White *et al.* 1992).

Thus, the original spatial resolution of the initial data sets varies with region, although all data are represented on the same $1^\circ \times 1^\circ$ grid. This resolution is only reasonable in areas of central and northern Eurasia as well as in most of North America, while the rest of the world is more probably characterized by a $5^\circ \times 5^\circ$ resolution.

The estimation of the thermal state and resulting density of the oceanic lithosphere was based on the digital ocean-floor age grid (Müller *et al.* 1993) derived from magnetic anomaly analyses. For the continental areas a maximum age of 200 Ma was simply assumed as an initial approximation.

3 GRAVITY FIELD OF THE ISOSTATIC LITHOSPHERE MODEL

3.1 General problems with the isostatic correction of observed gravity and geoid

Long-wave free-air anomalies and geoid undulations are often used for investigations of the Earth's deep structure and global dynamic processes. However, the lithosphere structures (even fully isostatically compensated) may create long-wave gravity field and geoid variations which exceed in magnitude the deep and dynamic e ects (e.g. Chase & McNutt 1982; Hager 1983; Artemjev *et al.* 1994). Until now, gravity and topography have been the only surface observations with a nearly complete global coverage for use in lithospheric studies. Thus, it is necessary to use some general concept to reproduce and to remove the lithosphere e ect from the observed gravity. An isostatic condition according to which the total sum of anomalous masses above the level of compensation is equal to zero is a possibility.

Several attempts have been made to remove the influence of isostatically compensated lithosphere in the global gravity field. For oceanic areas di erent types of the well-known cooling lithosphere model were used (e.g. McKenzie 1967; Davis & Lister 1974; Lister 1982; Hager 1983; Cazenave *et al.* 1986). Despite some variations, applications of this model may be divided into two classes. In the simple plate model, the temperature is assumed to be constant at some depth of the order of 120 km (Turcotte & Oxburgh 1967; Davis & Lister 1974), whereas in the simple boundary-layer (half-space) model the upper mantle is assumed to cool by conduction (Langseth *et al.* 1966; McKenzie 1967; Sclater & Francheteau 1970). These models may reveal di erences for lithosphere older than 120–150 Ma, but until now these di erences have not been recognized when analysing experimental data (Parsons & Sclater 1977). For making the isostatic correction, sea-floor age maps based on the interpretation of linear magnetic anomalies were used in some of the papers mentioned above (e.g. Cazenave *et al.* 1986). The cooling model reflects the general properties of the ocean structure but this is often disturbed by other processes and individual structures of di erent origin. The huge positive anomaly in topography,

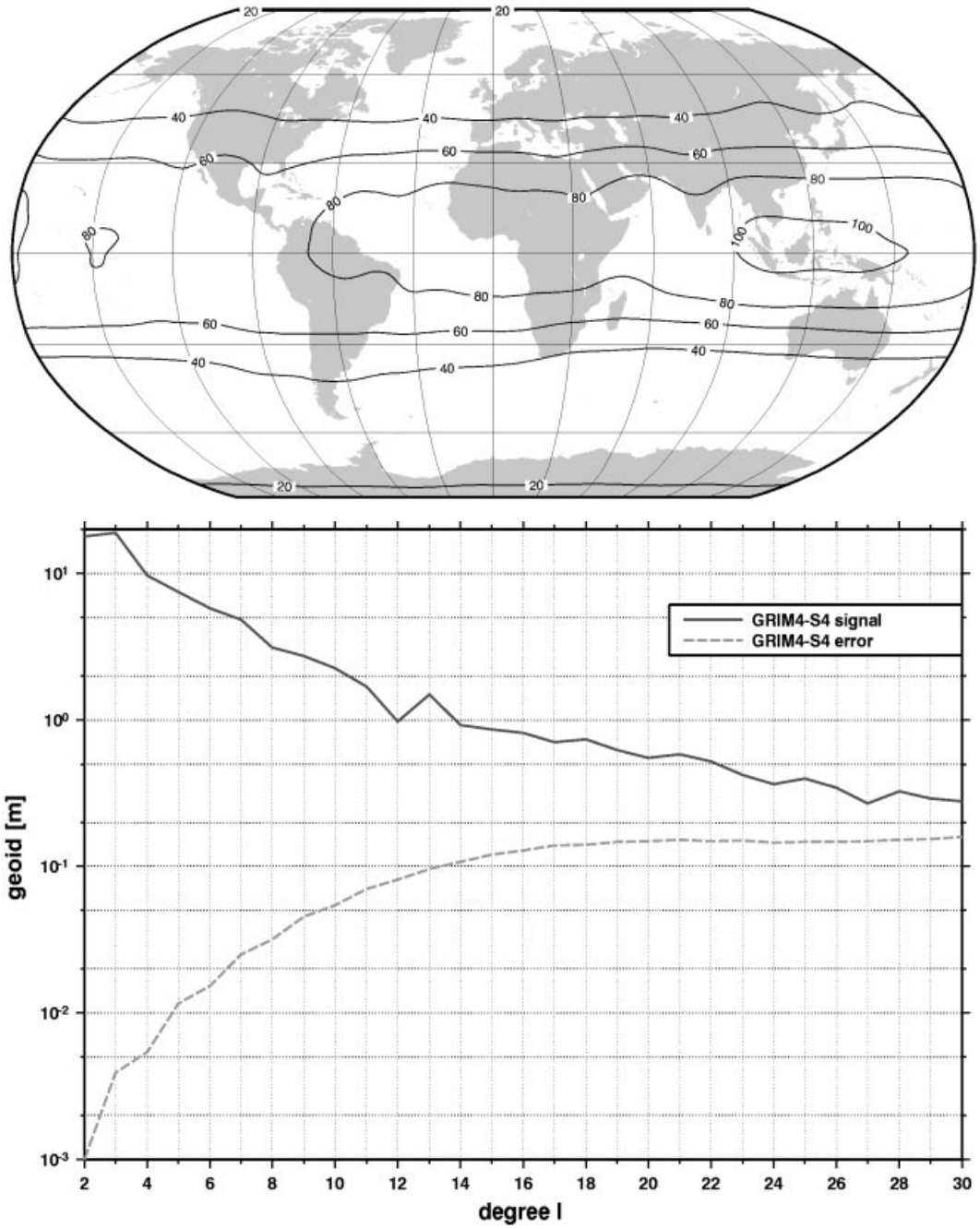

Figure 1. GRIM4-S4 geoid standard deviations: (upper) spatial distribution (commissioning error up to degree and order 30), unit: cm; and (lower) square root of error and signal degree variances, unit: m.

gravity and geoid located over the North Atlantic is one of the most striking examples. Thus, removing only the predicted ocean topography and its compensation, the residual gravity and geoid still contain anomalous lithospheric signals which mask the dynamic e ects and the impact of deep structures.

Chase & McNutt (1982) spread masses to compensate ocean topography in a vertical column down to a depth of 100 km. For continents they assumed the well-known Airy scheme and used an approximation concentrating all compensating masses in a thin layer at a depth of 35 km, which is the generally accepted value for continental crustal thickness. Pavlis & Rapp (1990) used the Airy–Heiskanen model for the whole Earth including oceans. Sünkel (1986) applied the linearized Vening Meinesz isostatic model and determined both depth to the compensation level and a smoothing factor to account for a regional compensation. Sünkel analyzed the geoid–topography transfer function up to degree 180 and deduced on a global scale a depth to the compensation level of 24 km. These models are isostatic, but they do not explain di erences for specific tectonic regimes. Recent geophysical studies show that density

variations in the upper mantle play an important role in the compensation of global crustal structures (Artemjev & Kaban 1986; Artemjev *et al.* 1994; Mooney *et al.* 1998). This conclusion follows from the well-known fact that the average position of the Moho discontinuity is di erent for di erent areas; for example, for western Europe, eastern Europe and the east Siberian plate such di erences exceed 25 km (Belousov 1987). It was also shown that not more than 65 per cent of the isostatic compensation of regional structures in northern Eurasia may be explained by Moho variations (Artemjev *et al.* 1994; Artemjev & Kaban 1994). This may shift depth to the e ective compensation level by a factor of 2 and causes remarkable changes in the model gravity field or geoid. In the present study we try to take into account such di erences on a global scale.

The approach of Le Stun & Ricard (1995) is similar to that used in the present paper. These authors used data on crust and sediment thickness and determined the density structure and thickness of the lithosphere. Using least-squares inversion, Le Stun & Ricard tried to fit both the observed geoid and the topography on a global scale using an isostatic balance condition. The di erence between observed and predicted topography was regarded as 'non-isostatic'. On the base of this result, a geodynamic conclusion was made: continents and ancient cratons are well compensated and non-isostatic topography is possibly much lower than predicted from mantle flow models (e.g. Forte *et al.* 1993; Hager & Clayton 1989). Thus, multiparameter models to determine simultaneously the density structure of the crust and upper mantle and mantle dynamics give unstable results depending on the approach used. Also, the idea of constructing a lithospheric model with the same density parameters for the whole Earth does not fit with present-day knowledge (e.g. Mooney *et al.* 1998). Most of the crustal density parameters may be determined independently from gravity data analyses giving more stability to subsequent determinations of problematic mantle parameters. It is also noteworthy that Le Stun & Ricard constructed the isostatic model by fitting observed and predicted gravitational model spherical harmonic coe cients obtained for the whole Earth, whilst in reality every lithospheric density inhomogeneity and individual structure contributes to all geoid coe cients, and aliasing may occur.

In this study the gravitational e ects of crustal and upper-mantle inhomogeneities are subtracted from the observed gravity and geoid in a multistep approach: (1) the contribution of the crust is determined based on available density, topography and Moho depth data; (2) the contributions of the oceanic lithosphere temperatures and thus density anomalies are determined according to the well-constrained cooling ocean model; and (3) additional compensating masses are assumed and estimated to provide isostatic compensation of the residual unbalanced masses after having performed steps (1) and (2). After subtraction, the resulting isostatic anomalies will then primarily reflect dynamical and deep e ects.

3.2 Residual topography, gravity field and geoid

The residual topography (p) for each $1^\circ \times 1^\circ$ spherical column is determined using the following formula:

$$p = (\rho_{\text{top}}/2.67)t_{\text{obs}} + \frac{1}{2.67}\int_0^L \Delta\rho(h)\left(\frac{R-h}{R}\right)^2 dh, \qquad (3)$$

where ρ_{top} is the e ective density of positive topography, t_{obs}—2.67 g cm^{-3} is the normal value for continents and 0.92 g cm^{-3} for ice, h is the depth with respect to the geoid, $\Delta\rho(h)$ is the anomalous density (including water) relative to the density in the reference model as defined below, L is the lower bound of the density distribution considered and R is the radius of the Earth.

The oceanic lithosphere reference model used here is derived from the density distribution in an old 'normal' ocean with an age of 200 Ma. The column includes 6.4 km of water with a density of 1.035 g cm^{-3}, a 7.2-km-thick crust with a constant averaged density of 2.85 g cm^{-3} and an upper mantle where the density corresponds to the plate model of the cooling oceanic lithosphere. The mantle density profile for an ocean floor at time t is then determined according to the following equation (Hager 1983):

$$T(h,t) = T_0\left\{\frac{(R-L_{\max})h}{(R-h)L_{\max}} + \frac{2R}{(R-h)\pi}\sum_{n=1}^{\infty}\frac{1}{n}\sin\left(\frac{n\pi h}{L_{\max}}\right) \times \exp(-n^2\pi^2 k_t t/L_{\max}^2)\right\}, \qquad (4)$$

where $\rho(h) = 3.3$ g cm^{-3} $[1-\alpha T(h,t)]$, with $\rho = 3.3$ g cm^{-3} being the density of mantle rock at 0 °C, $L_{\max} = 120$ km is the depth, where $T_0 = 1300$ °C (maximum thickness of the lithosphere), $k_t = 10^{-6}$ m^2 s^{-1} is the thermal di usivity, h is the depth with respect to the seafloor, t is the age, $\alpha = 3.3 \times 10^{-5}$ °C^{-1} is the volume coe cient of thermal expansion, T is temperature, and R is the radius of the Earth.

This equation is used to estimate upper-mantle density in the ocean regions down to 120 km below the seafloor according to the age map derived from magnetic anomalies (Müller *et al.* 1993). Seafloor depth for each column results from the condition that the masses must be in balance with the 200 Ma reference column. For the continents we simply assume from the beginning that the upper mantle is homogeneous with the same density distribution as in the reference model ($t = 200$ Ma); the residual topography and gravity will then indicate possible perturbations to this initial model. The thickness of the reference continental crust, which is in a balance with old ocean lithosphere, must be equal to 39.64 km, assuming zero topography and a constant averaged crustal density of 2.85 g cm^{-3}.

There exist other equivalent parametrizations such as residual topography and characterizing the internal 'self-compensation' of the density inhomogeneities. One example is the so-called 'free' mantle surface introduced by Artemjev & Kaban (1986). The definitions di er only by a scaling factor. The definition (3) seems to be close to that applied by Mooney *et al.* (1998), though these authors do not give the exact formula or the parameters of the reference model. A variation in the arbitrary reference density model a ects only the constant level of the residual topography and gravity (Hager 1983).

The residual topography, calculated according to eq. (3) and using the initial crustal data as described in Section 2.3, is shown in Fig. 2. It is truncated after degree 30 of its spherical harmonic expansion to exclude small-scale features which are not trustworthy in some of the initial data sets. As a result of the accuracy of the initial crustal data (Mooney *et al.* 1998; Artemjev *et al.* 1994), the large-scale residual topography is accurate to ± 0.4 km in the well-studied areas (North America, northern Eurasia and some of the oceanic regions); in the

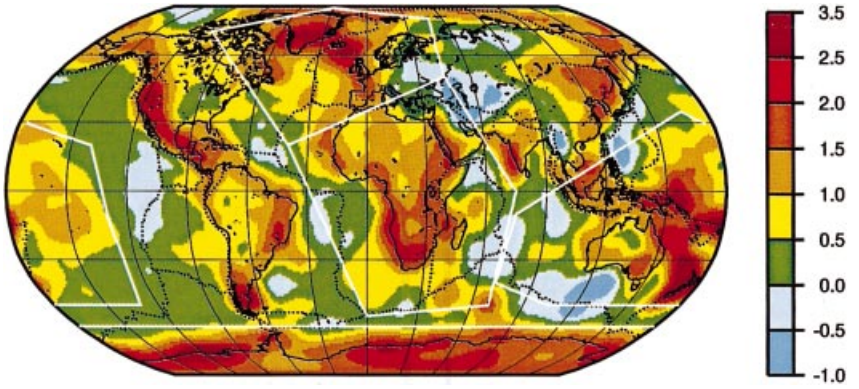

Figure 2. Residual topography (unit: km) after removal of topographic e ects computed from data on the crustal density structure and on mantle density anomalies according to ocean-floor age data and the cooling oceanic lithosphere model (all continental areas are adjusted to the same age of 200 Ma). The zero level corresponds to the 'normal' old ocean. The residual topography is connected with anomalous mantle structure and dynamic e ects. The boundary lines indicate the main anomalous tectonic structures which are the subject of later gravity–topography admittance calculations.

remaining areas, where the crustal data are partly interpolated, this uncertainty may increase to ± 0.8 km. The only exception is the Antarctic region, where the initial crustal data are almost everywhere predicted and possible errors are hard to estimate, thus analysis results for Antarctica are probably not reliable.

The most important characteristic of the map shown in Fig. 2 is that the residual topography has a positive o set of 0.8 km and varies from -1 km to 3.2 km. Besides the inaccuracy inherent in the initial data sets, residual topography may arise from two factors: one, which will be discussed later, is dynamical support by mantle flow; the other is due to unmodelled upper-mantle density inhomogeneities compensating the residual topography. Lower-than-average upper-mantle densities support positive residual topography and vice versa (Artemjev & Kaban 1986; Mooney *et al.* 1998; Vidale & Mooney 1998). Thus, considering the on average positive residual topography, the standard density distribution in the old ocean mantle may be taken as an upper limit. The age-dependent e ect of the cooling lithosphere is already modelled in the residual topography; that is, the entire ocean is adjusted with respect to the same 200 Ma old reference column. Note that over most of the ocean area, variations of residual topography are small and are close to those over the main continental cratons in northern Eurasia and North America. This means that the di erent temperature conditions between these marine and continental regions must be compensated by a di erence in the chemical composition of the upper mantle: depleted mantle under the Precambrian cratons is significantly lighter than non-depleted oceanic mantle at the same temperature. This conclusion agrees with the results of petrological studies (e.g. Jordan 1981, 1988), which suggest that temperature and composition e ects neutralize each other in density under old continental areas. These results do not agree with the studies of Mooney *et al.* (1998) and Vidale & Mooney (1998), who found that, unlike in oceanic areas, the topography is significantly lower than predicted over Precambrian cratons. This discrepancy in the pattern of residual isostatic topography probably results from di erences in the reference models used and partly from the initial data sets, which are improved in the present study for northern Eurasia.

There exists a system of high positive anomalies in residual topography, indicating potential areas for an anomalously low-density upper mantle and/or dynamic support. Three global maxima with a characteristic extent of 3000 km or more can be recognized: the North Atlantic, eastern Australia–SW Pacific and Africa. Their amplitudes exceed 2 km and are significantly larger than possible modelling errors. A relatively narrow band (about 1000–1500 km wide) of positive anomalies in the residual topography is observed west of North America, continuing over central America and then moving to the east of South America. A relatively small but distinct maximum is located over the southwestern part of India and the adjoining ocean.

The origin of the residual topography may be to a certain extent resolved by computing the residual gravity and geoid using the same data sets as for the residual topography. If an anomaly in residual topography can even partially be attributed to mantle density inhomogeneity, then the residual gravity and geoid should reveal anomalies of an opposite sign over such a structure.

The gravity e ect of topography, crust and upper mantle was calculated as a 3-D direct gravity problem solution on a spherical earth taking into account changes in anomalous density in the horizontal and vertical directions and the surface elevation referenced to the geoid. The earth's surface, crust and upper mantle were divided into cells on a $1^\circ \times 1^\circ$ geographic grid, as described above. Horizontal layer boundaries within each cell correspond to the boundaries of the anomalous layers. The predicted gravity at each point is determined as a sum of the anomalous gravity created by all the spherical elements distributed over the earth. The calculation method is the same as in Artemjev *et al.* (1994) and is based on the formulae published in Strakhov *et al.* (1989). The gravity disturbance is defined as the di erence between observed gravity and predicted gravity.

We use a spherical harmonic expansion to convert calculated residual gravity disturbances into residual geoid undulations. The corresponding relation of the spherical harmonic coe cients is as the follows (Heiskanen & Moritz 1967):

$$\delta g(\Theta, \lambda) = \frac{1}{R} \sum_{l=0}^{\infty} (l+1) T_l(\Theta, \lambda), \qquad T(\Theta, \lambda) = \sum_{l=0}^{\infty} T_l(\Theta, \lambda),$$
$$N(\Theta, \lambda) = T(\Theta, \lambda)/\gamma(\Theta, \lambda), \tag{5}$$

where $T(\Theta, \lambda)$ is the disturbing gravitational potential, $T_l(\Theta, \lambda)$ is the Laplace's surface harmonic of degree l, R is the equatorial radius of the Earth, $\gamma(\Theta, \lambda)$ is normal gravity, $\delta g(\Theta, \lambda)$ is the gravity disturbance and $N(\Theta, \lambda)$ is the geoid undulation. The residual gravity and geoid have been computed in two steps. In the first only the e ect of the crust according to the adopted crustal model has been removed. The upper mantle was everywhere considered to be horizontally homogeneous as in the reference model. The resulting (mantle) gravity disturbances and geoid undulations are shown in Figs 3(a) and (b), respectively. These anomalies were centred by removing the overall mean value. This mean value is of no importance because if one removes some anomalous masses which are non-zero on average for the whole Earth, the constant level of the residual field will be shifted depending on the total amount of these masses but not on the specific density structure under the point. The residual gravity is estimated to be accurate to within ± 40 mgal in the well-studied areas (the same as for the residual topography); for the rest of the world possible errors may reach 80 mgal. The fields in Fig. 3 are truncated after degree 30, as was done with the residual topography. These maps represent an intermediate step of the isostatic modelling, but a comparison with seismic tomography results, which reflect the complete mantle e ect, is meaningful. The system of negative anomalies connected with ocean spreading centres is one of the most visible patterns in Fig. 3.

In the second step, the gravity e ect of cooling oceanic lithosphere is also computed and is removed from the mantle anomalies of the first step. The result is shown in Fig. 4(a) in terms of gravity disturbances and in Fig. 4(b) in terms of geoid undulations. These fields reflect disturbances with respect to a homogeneous continental mantle and to 'normal' oceanic lithosphere, whose density properties depend only on its age. Both maps are centred by removing the constant component and are truncated after degree 30 of their spherical harmonic expansions. The geoid undulations are smoother than the gravity and reflect only the large-scale or high-amplitude small-scale features. The main features of both residual gravity and geoid correspond (with an opposite sign) to the pattern of the residual topography, supporting the idea that at least part of its variations are explained by upper-mantle density variations. In some places density anomalies in the mantle exist together with up-/downwelling mantle flow. In this case some part of the residual topography is explained by mantle dynamics. A joint analysis of the amplitudes of the corresponding topographic and gravity fields and an isostatic adjustment may resolve to a certain extent the relation between the various e ects. These steps are performed in the following sections.

3.3 Isostatic model of the lithosphere

As taking into account the flexural rigidity of the lithosphere is not necessary for a long-wave isostatic model, we assume a local compensation condition, which may be written on the sphere as follows (Hager 1983):

$$\int_t^{H(\varphi,\lambda)} \Delta\rho(h)\left(\frac{R-h}{R}\right)^2 dh = 0, \qquad (6)$$

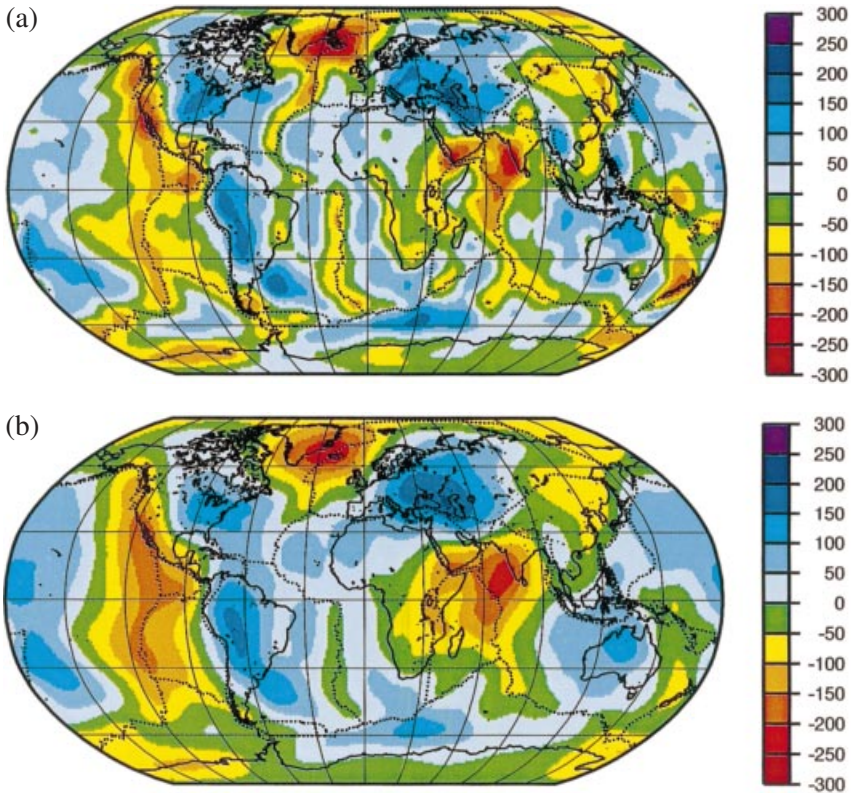

Figure 3. Residual gravity (unit: mgal) and geoid (unit: m). The e ect of the crustal density structure based upon the continental crustal database is removed from observed gravity disturbances (a) and geoid undulations (b). Both fields are centred by removing its average value and truncated after degree and order 30.

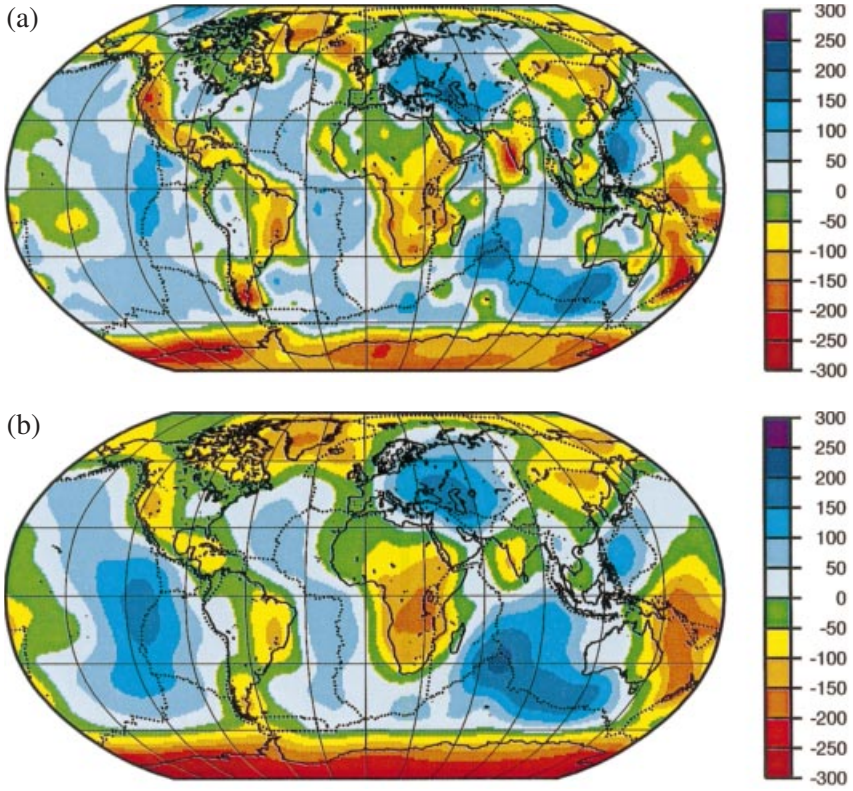

Figure 4. Residual gravity (unit: mgal) and geoid (unit: m) obtained after additionally removing from the fields in Fig. 3 the gravitational e ect of the cooling oceanic mantle determined from ocean-floor age data. The residual gravity disturbances (a) and geoid undulations (b) are centred by removing its average value and truncated after degree and order 30.

where $H(\varphi, \lambda)$ is the depth to the compensation level from the geoid, t is the topography and the other parameters are as defined in eq. (3).

Following this definition, the depth to the compensation level may be di erent in di erent areas. This level should be placed somewhere in the asthenosphere, and the above equation includes the possibility that variations of the depth to the asthenosphere may exceed its thickness. Here we use a mechanical asthenosphere definition as a low-viscosity layer. Another important thing which is stressed by this equation is that it defines the isostatic condition of the lithosphere relative to the geoid. Thus specific corrections accounting for masses between the geoid and the reference ellipsoid as described in Chapman & Bodine (1979) are not necessary.

Condition (6) corresponds to the above definition of the residual topography (3), which should be equal to zero if the density inhomogeneities in every vertical column compensate each other. When computing isostatic anomalies of the gravity field, additional compensating masses equal to the residual topography but with an opposite sign (not taking into account the spherical term) are placed somewhere within the Earth. The origins of these masses are quite di erent, and in many places they are a subject for discussion, but their distribution may be characterized by one parameter, which is the only important parameter for a large-scale isostatic model gravity field: the e ective depth (Z) to the centre of the compensating masses, $\Delta\rho_c$ (e.g. Sünkel 1986):

$$Z = \int_{L_1}^{L_2} h\Delta\rho_c(h)dh \Big/ \int_{L_1}^{L_2} \Delta\rho_c(h)dh, \tag{7}$$

where L_1, L_2 indicate the lower and upper boundaries of the compensating mass distribution.

This expression has an analogy with the well-known simplified expression for the geoid undulation caused by an anomalous density distribution ($\Delta\rho$) (Ockendon & Turcotte 1977; Haxby & Turcotte 1978):

$$N = -\frac{2\pi\mathcal{G}}{\gamma} \int_{L_1}^{L_2} h\Delta\rho(h)dh, \tag{8}$$

where $\mathcal{G}$ is the gravitational constant and γ is normal gravity at the Earth's surface.

Thus, any compensating model may be approximated by a thin layer placed at the e ective compensation depth where all compensating masses are condensed. This depth may be specified in its spatial distribution using the well-known admittance technique based on the cross-spectral analysis of the gravity field—here the residual gravity disturbances—and external load—here the residual topography. It may be assumed in the same way as suggested by e.g. Dorman & Lewis (1970) for Bouguer gravity and topography that the residual gravity disturbances may be represented as a convolution of the residual topography p and some function f, named a transfer function or admittance:

$$\Delta g = f * p + \varepsilon, \tag{9}$$

or in the spectral domain:

$$G = FP + \mathrm{E}, \tag{10}$$

where ε is a 'noise' component not correlated with the load. Each specific isostatic model has its own admittance, thus

when determining this function from experimental data, it is also possible to draw some conclusions about the isostatic compensation mechanism for the area under investigation. For the e ective layer model described above it may be written as follows (plane case):

$$F = -2\pi\mathscr{G}\rho\, \mathrm{e}^{-kZ}, \tag{11}$$

where, $k = \sqrt{k_x^2 + k_y^2} = 2\pi/L$, L is the wavenumber, Z is the compensation depth, $\mathscr{G}$ is the gravitational constant and ρ is the density of the residual topography. The admittance is usually determined as the real part of the gravity–topography cross-spectrum divided by the power spectrum of the load (topography):

$$F(k) = \mathscr{R}e\langle G(\mathbf{k})P^*(\mathbf{k})\rangle / \langle P(\mathbf{k})P^*(\mathbf{k})\rangle, \tag{12}$$

where the angle brackets indicate averaging over the discrete wavenumber bands to reduce the noise influence. Here a modified method developed to determine experimental admittances for particular structures on the sphere is applied, which is explained in the Appendix.

Corrected experimental admittances for the main tectonic structures are shown in Fig. 5. Coherence spectra of residual topography and gravity result in values between 0.9 and 1 for wavelengths greater than 700 km except for the North Atlantic, where the coherence values range from 0.8 to 0.9. We compare the global admittance relation, obtained for the whole Earth, with those for the most pronounced features visible in the residual topography. The most pronounced are the northern and southern hemispheres characterized by the domination of continental and oceanic structures, respectively. Both hemispheres were bounded at 60° latitude because the initial data for near-polar areas are less reliable. The four most pronounced maxima of the residual topography are located over the north Atlantic, Africa, Australia–SW Pacific and Antarctica. The boundaries of these areas are shown in Fig. 2. With this study being limited to a global scale, smaller-scale features are left for further analysis.

The experimental values were analysed in the wavelength interval 900–3000 km to find the best value for the depth to the e ective compensation layer. The lower value of this wave band is given by the resolution of most of the initial data sets, while the upper bound fits the extension of the four areas shown in Fig. 2. Also, for wavelengths longer than 3000 km the influence of very deep-seated density inhomogeneities or mantle dynamics may dominate. This is demonstrated by some of the admittance graphs shown in Fig. 5, where the admittance characteristics for wavelengths greater than 2500–3000 km are remarkably di erent from those for smaller wavelengths. For almost all admittances the estimated uncertainty of the experimental values is much larger for the long wavelengths than for the shorter ones, which indicates that there exist large-scale components in the residual gravity which do not correlate with near-surface structures reflected in the residual topography. There exists also a systematic decrease of the absolute admittance values at long wavelengths (about 20–25 per cent for the North Atlantic), which is evidence either for a dynamical support of some part of the residual topography or for super-deep compensation of these structures at a depth of about 200 km or more.

Comparing the experimental admittances with the synthetic calibration lines (see the Appendix) at adopted compensation levels of 25, 50 and 75 km depth, the following conclusions can be drawn.

(1) The 25 and 50 km depths approximately represent the upper and lower bounds of the e ective compensation layer. Despite some scattered values, all admittance curves shown in Fig. 5 are between the corresponding calibration lines for the wavelength interval 900–3000 km. This means that the main sources of the additional masses compensating the residual topography are located in a subcrustal layer and are due to density inhomogeneities of the uppermost mantle.

(2) A remarkable di erence in the e ective compensation depths in the northern and southern hemispheres, 50 and 37 km, respectively, was found. This di erence may be explained for the most part by the di erence in the average crustal thickness if one adopts the previous conclusion about the upper-mantle origin of the additional compensating masses. According to the underlying data sets, the average depth to the Moho in the northern hemisphere (below 60°N, the boundary of the admittance calculations) is 24.4 km, whereas in the equivalent part of the southern hemisphere the averaged Moho depth is 16.4 km.

(3) The admittances obtained for Africa and Antarctica are unrealistic: for the wavelength interval 900–3000 km their values suggest that all compensating masses are placed at zero depth. This means that the initial data on the crustal structure over Africa and Antarctica are not accurate enough for use in this analysis.

(4) The results obtained for the North Atlantic maximum and for Australia–SW Pacific in general fit those obtained for the whole northern and southern hemispheres, respectively, which is not surprising because these features provide the main signal for both residual gravity and topography.

As a result of these conclusions, additional masses compensating the residual topography were placed in the uppermost mantle between the Moho and 70 km depth. The density variation in each $1° \times 1°$ column of this layer was determined in such a way that the anomalous masses exactly balanced the residual topography at the Earth's surface. The middle of this layer fitted the e ective compensation depth within a reasonable limit: 47 km instead of 50 km (northern hemisphere) and 43 km instead of 37 km (southern hemisphere), on average. In spite of the somewhat larger value in the southern hemisphere, it was decided to use the same model for the whole Earth because 6 km is well within the estimation error and is insignificant for gravity modelling. To be more realistic, the maximum density variation in the upper mantle was restricted to a maximum of 0.1 g cm^{-3}, but, where necessary, the thickness of the anomalous upper mantle layer was increased. Using this procedure it was found that the maximum depth to the bottom of the compensation was 118 km under Tibet, and the average e ective compensation depth was increased to 49 km in the northern hemisphere.

3.4 Isostatic anomalies of the gravity field and geoid

The gravitational impact of the additional compensating masses was estimated in the same way as for the initial fields described in Section 3.2 and added to the gravity of the initial lithosphere model. The total gravity of the self-compensated crust–upper-mantle model was obtained in terms of free-air

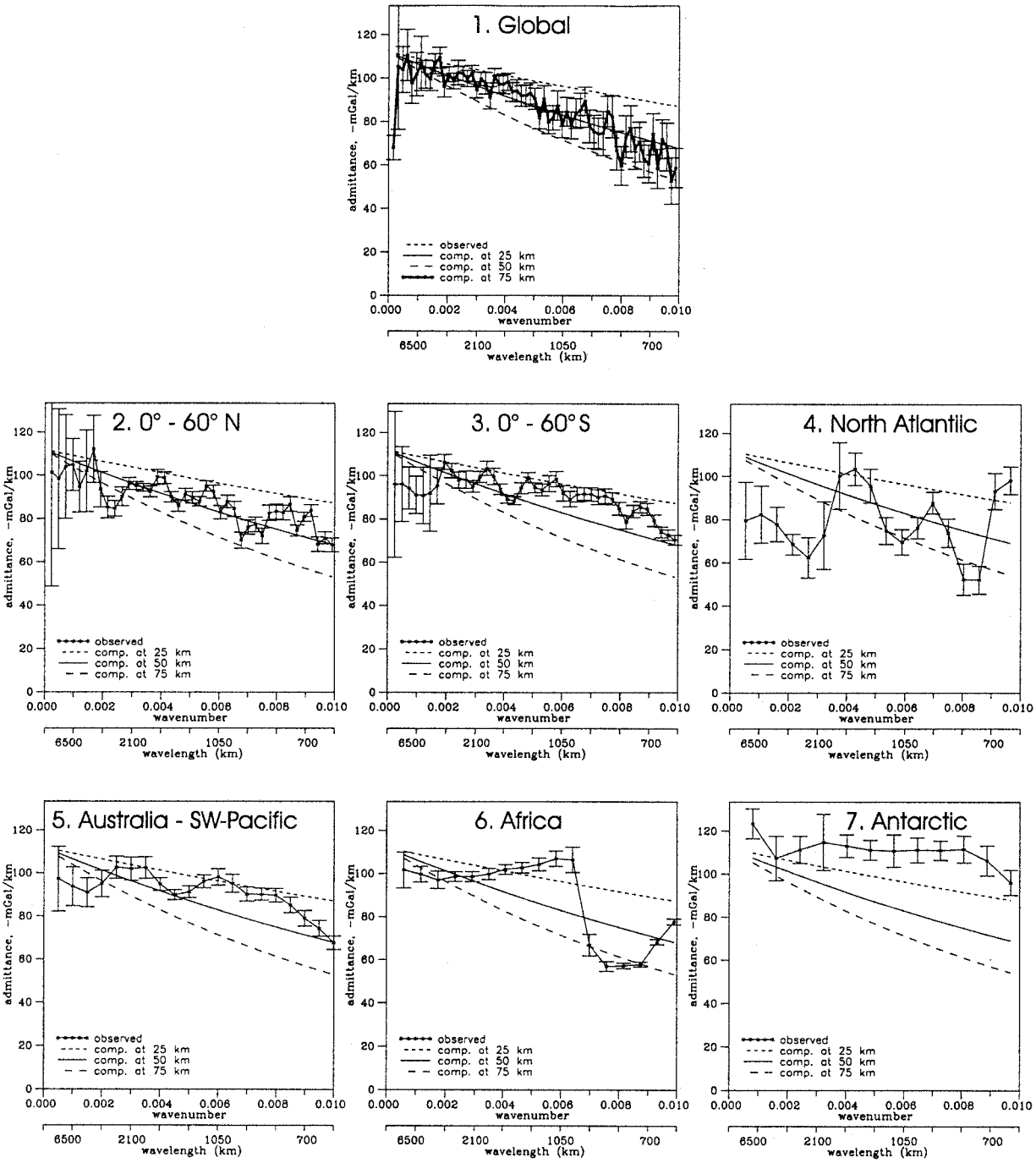

Figure 5. Experimental admittances obtained from the residual gravity disturbances (Fig. 4) and residual topography (Fig. 2). The global admittance is determined directly from spherical harmonic coe cients. The admittances for parts of the Earth and tectonic regimes are computed applying the approach as described in the text. Smooth curves correspond to 'ideal' admittances concentrating all compensating masses in a thin layer at depths of 25, 50 and 75 km.

gravity disturbances, as shown in Fig. 6(b). Removing this field from the observed free-air disturbances (Fig. 6a) yields the isostatic gravity disturbances (Fig. 6c). The gravity of the total isostatic model is compared to that of the initial residual fields less influenced by errors in the initial crustal data because shortcomings are balanced by opposite compensating masses, although these are placed at greater depths. Therefore, the fields given in Fig. 6 have the initial $1^\circ \times 1^\circ$ resolution of the input gravity data.

The gravity field of the isostatic model is converted into geoid undulations according to eq. (5) and taking into account a 'self-adjustment' of the internal gravitational potential. Since anomalous masses of the lithosphere change not only the external but also the internal gravitational potential, inner boundaries will be warped, producing additional anomalous potential and changing the shape of the geoid, thus provoking additional isostatic adjustment in the lithosphere. This process will be continued until equilibrium is achieved. The question

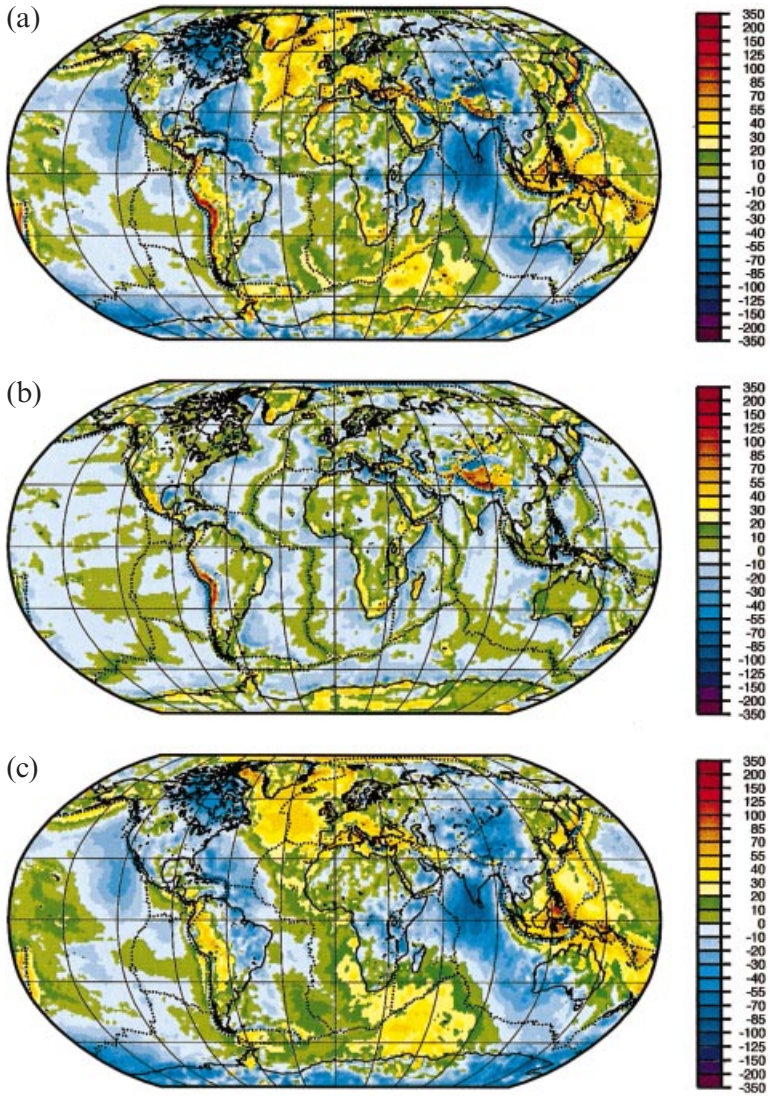

Figure 6. (a) $1^\circ \times 1^\circ$ averaged free-air gravity disturbances (unit: mgal) as implied by the EGM96 global gravity model. (b) $1^\circ \times 1^\circ$ isostatic lithosphere model gravity field (unit: mgal) representing the isostatically compensated crust and upper mantle. (c) $1^\circ \times 1^\circ$ isostatic gravity disturbances (unit: mgal) obtained after subtraction of the isostatic model gravity field in (b) from the observed free-air gravity disturbances in (a).

of how it will change the external potential is a classical geophysical problem (Vening Meinesz 1946). It can be solved in terms of Love numbers: if the original geoid undulation produced by the degree l of some isostatic lithosphere model is $\tilde{N}_l^{\mathrm{mod}}$ then the total geoid undulation will be (Hager 1983)

$$N_l^{\mathrm{mod}} = H_l \tilde{N}_l^{\mathrm{mod}}, \qquad H_l = \frac{l+0.6}{l}, \tag{13}$$

where H_l is the Love number for the correction of a potential of degree l. The geoid of the isostatic model (Fig. 7b) is subtracted from the observed one (Fig. 7a) to yield the residual isostatic geoid (Fig. 7c). The main statistical parameters of the observed, the isostatic model and the isostatic residual fields are listed in Table 1.

A comparison of the initial free air and the isostatic disturbances reveals a significant e ect when removing the influence of the isostatically compensated lithosphere from the observed gravity field. For example, the most pronounced continental free-air anomalies in the region of Tibet, in the Himalayas and in the Andes almost vanish in the isostatic gravity disturbance

Table 1. Main parameters of the observed, isostatic model and isostatic residual gravity field ($1^\circ \times 1^\circ$) and geoid (truncated after degree 30).

	Observed		Isostatic model		Isostatic residual	
	min, max	wrms	min, max	wrms	min, max	wrms
Gravity disturbance (mgal)	−303, +344	25.2	−186, +204	15.2	−205, +218	21.6
Geoid (m)	−103, +76	24.2	− 14, +44	5.1	−105, +71	25.0

wrms: weighted root mean square with weight equal to cosine of latitude of block value.

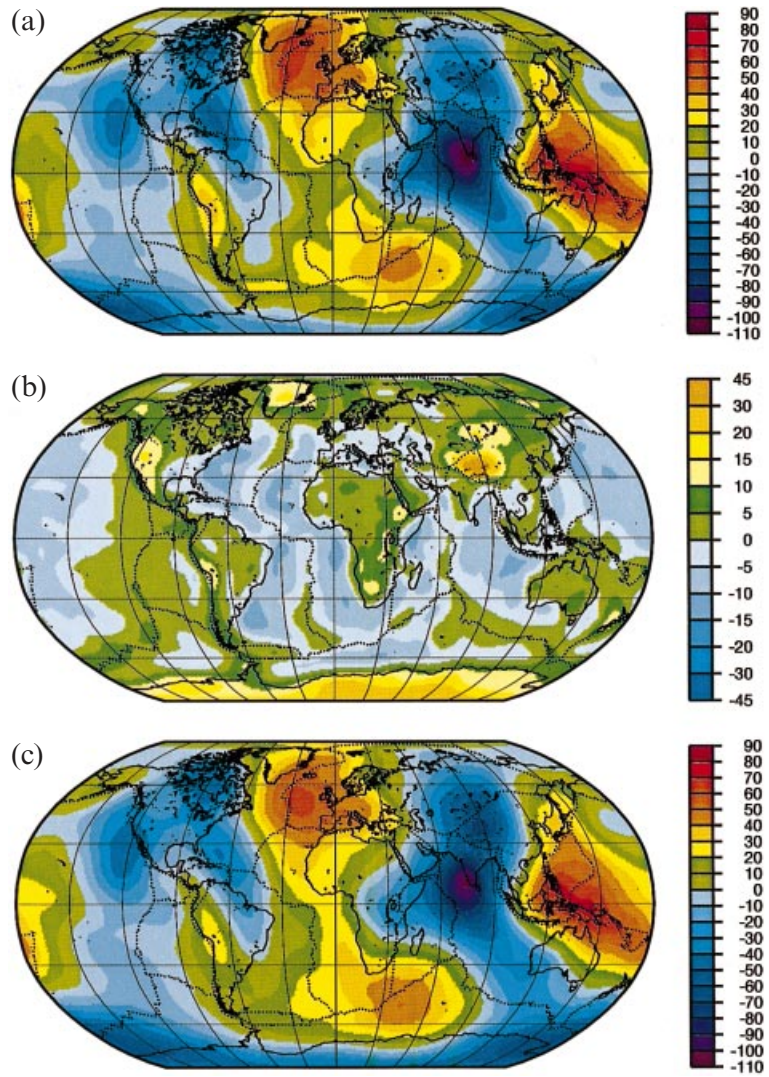

Figure 7. (a) Geoid undulations (unit: m) up to degree and order 30 as implied by the GRIM4-S4 satellite-only gravity field model. (b) Isostatic lithosphere model geoid (unit: m) up to degree and order 30 representing the isostatically compensated crust and upper mantle. (c) Isostatic residual geoid (unit: m) up to degree and order 30 obtained after subtraction of the isostatic model geoid in (b) from the observed geoid in (a).

map, and the high in free-air gravity along the North Atlantic Ridge changes into a widespread regional high in isostatic gravity disturbances. In general, one may conclude that the residual isostatic gravity is much less dependent on surface geology than on observed gravity. This is clearly seen at most of the continent–ocean transition zones, where the shift in gravity is significantly reduced by applying the isostatic correction. The signal degree variances according to eq. (2) of the isostatic gravity correction rapidly increase from degree 2 to degree 10, having the same minimum at degree 12 as in the observed spectrum (see Fig. 8).

In contrast, the signal degree variances of the isostatic model in terms of geoid heights reach a maximum at the lowest degrees and decrease quite smoothly towards the higher degrees. The overall signal amounts to more than 20 per cent of the observed geoid variations (see Fig. 9 and Table 1). At the same time, the correlation between the observed geoid and the geoid of the lithosphere model is not significantly di erent from zero (at the 95 per cent level) at lower degrees up to about degree 10 (Fig. 10). Therefore, the isostatic residual geoid is somewhat larger in amplitude than the observed one (25.0 m versus 24.2 m; see Table 1). The averaged signal of the geoid of the lithosphere model is about 1 m larger than for the models given in Le Stun & Ricard (1995) and Hager (1983). It should be noted that substantial parts of the observed geoid and of the long-wavelength gravity field reflect deep density heterogeneities and discontinuities not directly related to upper-mantle structure or dynamics. Thus, there exists a superposition of deep and near-gravitational e ects. This conclusion is confirmed by the admittance analysis results: the rapid increase of the uncertainty of most admittance values at the longest wavelengths may arise from the impact of deep mass anomalies being uncorrelated with residual topography. This conclusion emphasizes the importance of making the isostatic correction before interpreting the observed geoid and gravity with respect to deep mantle phenomena. The mixture of deep and near sources complicates the inversion of the observed geoid and gravity when solving for the upper-mantle and crust density structure.

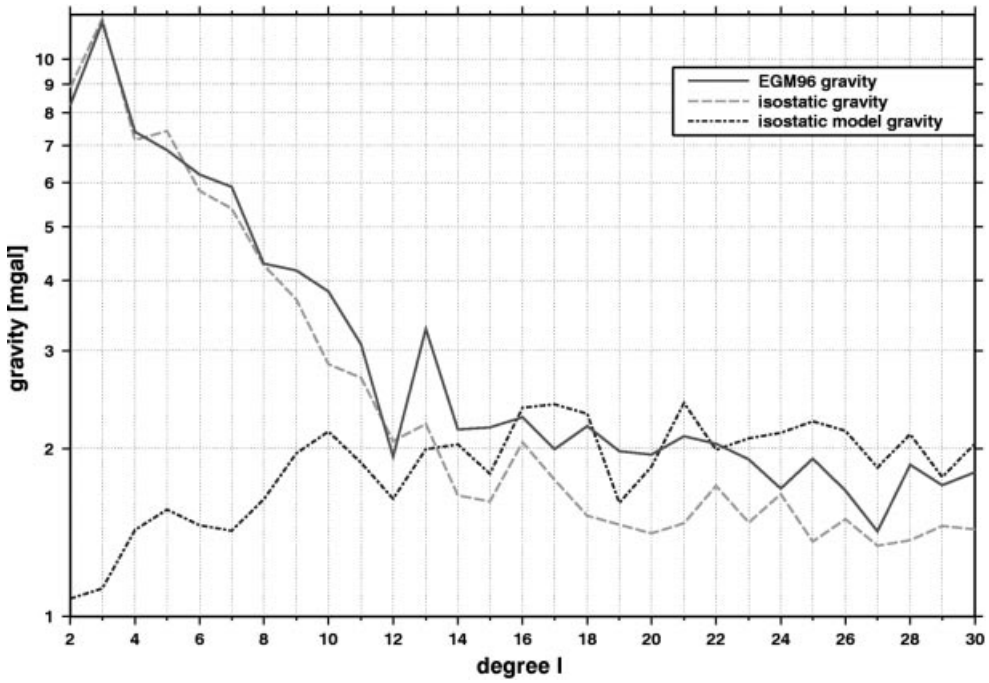

Figure 8. Square root of degree power spectra of observed (EGM96), isostatic model and isostatic gravity disturbances up to $l_{max} = 30$ (unit: mgal).

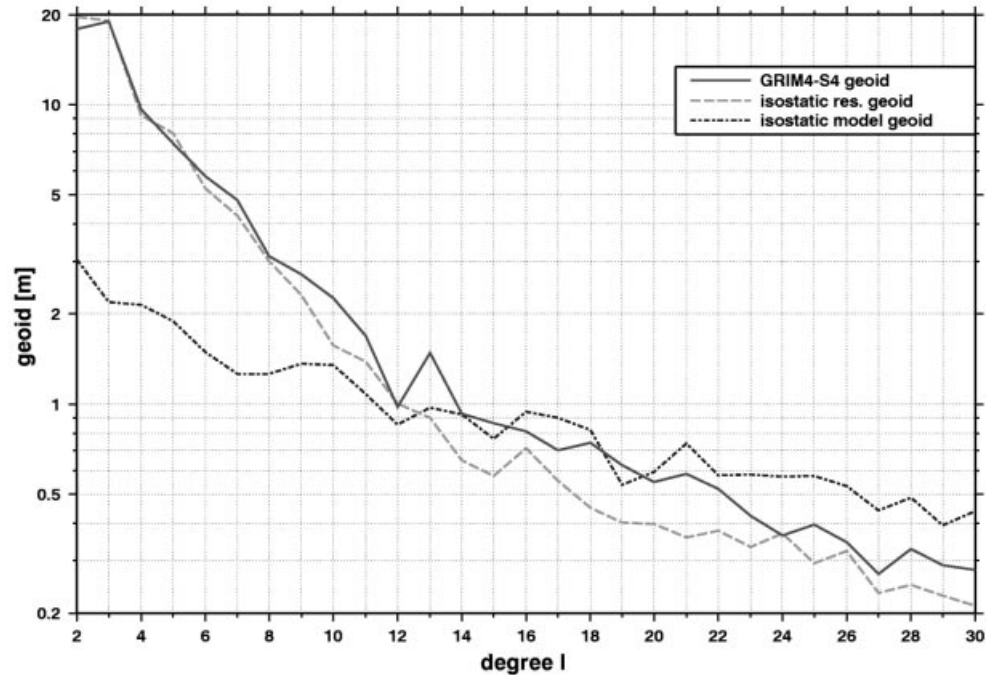

Figure 9. Square root of degree power spectra of observed (GRIM4-S4), isostatic model and isostatic residual geoid up to $l_{max} = 30$ (unit: m).

In general, it may be stated that most of the pronounced features being subdivided in the observed geoid become more continuous in the isostatic residual geoid. The most visible change is the confluence of three separate minima into one continuous minimum extending from the northeast Pacific over North America into the Caribbean basin. The same is true for the minimum extending from Siberia to western Australia via south India's super-depression, and, less visible, for the maximum extending from the North Atlantic southwards, almost to Antarctica.

4 DISCUSSION

4.1 Variations of the residual topography, residual and isostatic gravity and their relation to geodynamics

A joint analysis of the residual topography and residual and isostatic gravity provides a possibility of revealing and discriminating to a certain extent the e ects of upper-mantle density anomalies, mantle flows and deep density heterogeneities. Residual topography depends on both upper-mantle

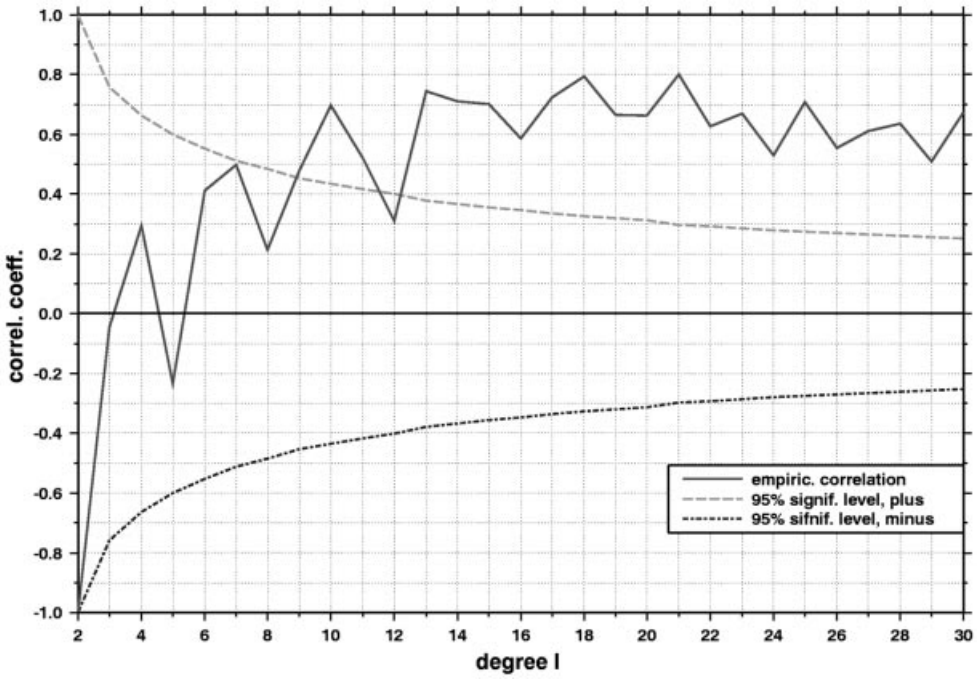

Figure 10. Degree correlation coe cients r_l between the observed and isostatic lithosphere model geoids and the 95 per cent significance level for r_l being significantly di erent from zero.

density heterogeneity and dynamical support, residual gravity is only sensitive to anomalous mantle density, while isostatic gravity anomalies are connected to deep density variations and dynamic e ects. Typical situations characterizing possible mutual relations and sources of these parameters are shown schematically in Fig. 11. These relations neglect the impact of deep mantle inhomogeneities and discontinuities on isostatic gravity, therefore any interpretation of features of the isostatic gravity field, as given below, is provisional.

Case A corresponds to the trivial situation when the crust and upper-mantle structure may be considered as completely predicted by the initial density model and, as a consequence, all residual fields and isostatic gravity are close to zero. This situation exists only in some oceanic areas where the process of 'normal' spreading is not influenced by additional processes.

Case B corresponds to a passive tectonic situation when the residual topography and the residual gravity are non-zero

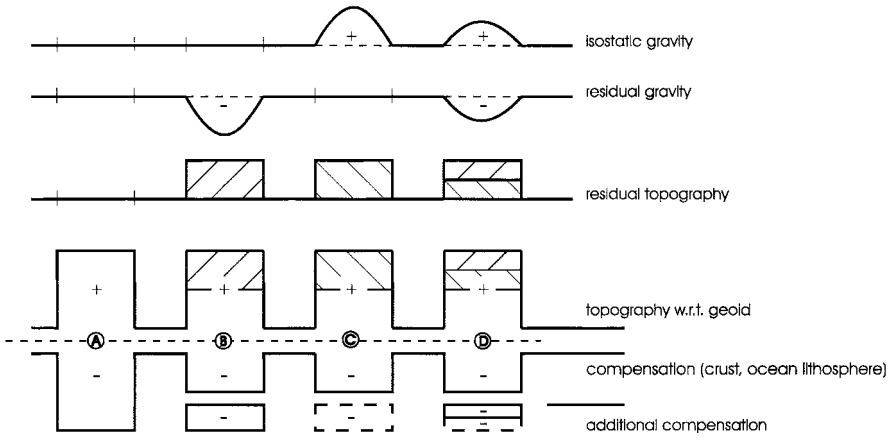

Figure 11. Typical tectonic situations, illustrating the relations between residual topography and residual gravity (i.e. before additional compensation) and isostatic gravity (i.e. after introduction of empirical additional compensation). Add a constant value to the isostatic gravity to obtain the assumed observed gravity. Situations are reversed for negative residual topography.

and of opposite sign because of an unknown mantle density inhomogeneity providing isostatic compensation. Isostatic gravity should be close to zero in this case because a dynamical e ect which disturbs isostasy does not exist. The band of positive residual topography west of North America may represent such a tectonic structure. The assumed negative density anomaly in the upper mantle seems not to be associated with dynamical support because there is no corresponding maximum in the isostatic gravity disturbances. A similar situation can be realized for Africa, but any conclusions are unreliable because of probable prediction errors and gaps in the initial crustal data sets. The global anomaly in the residual fields over the southwestern Pacific can be separated into two parts, of which the southern one may not be associated with a remarkable dynamical support.

Case C describes the situation where the lithosphere is shifted from its equilibrium state by forces not related to upper-mantle density inhomogeneities, the classical isostatic disturbance. This situation is typical of active plate boundaries, but associated variations in the residual fields are not visible because these phenomena are beyond the resolution of the initial data sets. The isostatic gravity disturbances of the $1^\circ \times 1^\circ$ resolution show these patterns, which are most visible at the boundaries of the west and north Pacific and at the African and Eurasian plate boundary. The pronounced negative isostatic gravity over Hudson Bay, Canada, is very probably connected with postglacial rebound (Simons & Hager 1997) and also the less pronounced minimum over Fenoscandia, but this e ect is too small to be detected in the residual topography.

Case D is a mixture of cases B and C; that is, it is a mantle density anomaly accompanied by additional forces. This situation is typical of upper-mantle dynamics. The most prominent example is the anomaly located over Iceland. This feature is characterized by a strong maximum in the residual topography, negative residual gravity and an isostatic gravity maximum, although this last component obviously consists of two parts: a smaller part located around Iceland and a wider part south of it, where no large topography was detected and which is therefore probably explained by large-scale and deep sources below the crust and upper mantle. Upper-mantle dynamics may also be responsible for the isostatic gravity maxima at the eastern boundary of Eurasia and northeast of Australia. A possible maximum in isostatic gravity over the 'hot' spot located southwest of India is completely masked by the huge global gravity minimum over this region.

4.2 Isostatic residual geoid and the deep structure of the Earth

It is emphasized in the previous sections that a considerable part of isostatic gravity disturbances is related to deep Earth structure and mantle dynamics. Due to their long-wavelength characteristics, these signals are more clearly visible in the isostatic residual geoid. Apart from some detailed features (e.g. the geoid high over western South America), the overall isostatic residual geoid exhibits some kind of a quadrupole structure. The main features of the isostatic residual geoid are much less related to near-surface structures than in the case of the observed geoid: significant shifts of the centres of highs and lows can be recognized when comparing Fig. 7(a) with Fig. 7(c), for example for the North Atlantic high and central Asian low. This evidence supports the idea of layered or at least partially layered mantle convection.

If the isostatic residual geoid reflects deep Earth structures and processes, it may be compared with results from seismic models of the Earth's mantle. The geoid signal arising from the Earth's deep interior is formed as a result of the interaction of mantle flow induced by density inhomogeneities and mantle discontinuity boundaries undulating as a result of this flow, as well as of the interaction at the core–mantle boundary. Because the complex geodynamic problem of a correct conversion of seismic velocities into densities is still unsolved, the main characteristics of seismic models and the residual isostatic geoid are compared only in the spectral domain. The relative power values per degree of a spherical harmonic expansion are then rather insensitive to errors in the applied density-to-velocity scaling. For the lower mantle the MDLSH model (Tanimoto 1990) of shear-wave velocity variations is taken for evaluation, assuming a constant density-to-velocity scaling of $0.2(\mathrm{kg\,m^{-3}})/(\mathrm{m\,s^{-1}})$ (Ricard *et al.* 1993). The estimation of the gravitational signal of the lower–upper-mantle transition-zone boundaries is based on the results of models B and C of Shearer (1993) using the PREM model (Dziewonski & Anderson 1981) values for the density contrast at these 410/660 km discontinuities. The gravitational signal to be expected from the core–mantle boundary was computed using the seismic model of Morelli & Dziewonski (1987), again adopting the PREM values for the density contrast.

Fig. 12 depicts the individual degree power spectra in terms of projected geoid undulations for the above-mentioned lateral

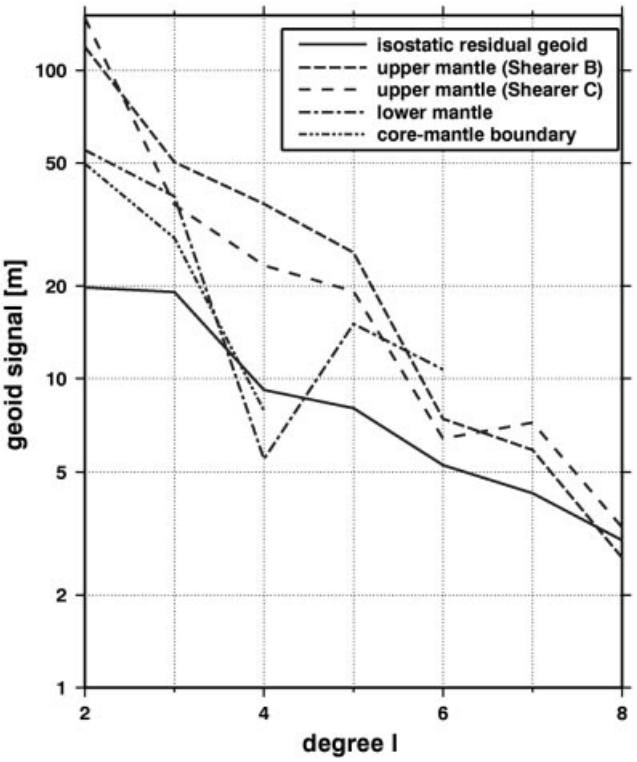

Figure 12. Comparison of square root of degree power spectrum of the isostatic residual geoid with those obtained for deep-seated inhomogeneities as implied by seismology and seismic tomography data (unit: m).

density variation models and the spectrum of the isostatic residual geoid. Some similarities can be detected in these spectra: the rapid decrease in power from degree 3 to 4 and from degree 5 to 6, which are enhanced in the isostatic residual geoid compared to the observed geoid, corresponds to spectral properties associated with the lower mantle and core–mantle boundary, and with the lower-upper-mantle transition zone boundaries, respectively. Thus, spectral features obtained in different studies based upon seismological data confirm the conclusion that the isostatic residual geoid reflects the integrated gravitational signal of deep-seated inhomogeneities and discontinuities more accurately than the observed geoid.

5 CONCLUSIONS

New global data on the density and structure of the Earth's crust, together with data on the age of the oceanic lithosphere, have been used to compute the gravity effect of the crust and oceanic lithosphere, which is then subtracted from the observed external gravity field and geoid. The residual gravity disturbances and geoid undulations reflecting the anomalous mantle structure have peak-to-peak amplitudes of about 500 mgal and 500 m, respectively. Almost no places with mantle denser than in the old 'normal' ocean were detected. This means that the remarkable differences between the thermal state of the continental and 'old' oceanic mantle must be compensated by differences in the chemical composition. Three global mantle anomalies are identified: North Atlantic, Africa and Australia–SW Pacific residual gravity minima. A relatively narrow band of negative residual gravity extends from northwest to southeast of the American continent.

The residual topography; that is, that part of topography which is not explained by the crustal and oceanic lithospheric data, has a peak-to-peak amplitude of about 4 km. These residuals are caused partly by unknown upper-mantle density inhomogeneities and partly by dynamical effects. The empirically found most appropriate model to compensate the mass of the residual topography for wavelengths from 900 to 3000 km implies additional density inhomogeneities in the upper mantle down to an average depth of about 70 km. Under the most pronounced crustal roots (e.g. Tibet and the Andes), the additional compensating masses may extend down to 120 km.

Based upon the initial data of the crustal and 'normal' ocean mantle structure and taking into account the empirical model of additional compensating masses, the gravitational effect of the isostatically compensated lithosphere has been computed and reduced in the observed gravity disturbances and geoid undulations. The resulting isostatic gravity disturbances based upon real lithosphere data are remarkably different from those implied by ideal isostatic models such as Airy, Pratt or Vening-Meinesz, which do not consider subsurface geology. The amplitudes of the isostatic gravity disturbances are significantly reduced compared to the observed field.

In contrast to the isostatic gravity disturbances, the isostatic residual geoid undulations are on average of the same amplitude as the observed ones. From this one may conclude that a substantial part of the geoidal and the long-wavelength gravity signals is due to deep density heterogeneities not directly related to upper mantle-structure or dynamics, which may be considered as a evidence for layered mantle convection. The spatial pattern of the geoid is also changed after the isostatic correction. Some features which are separated in the observed geoid are joined into global continuous lows and highs in the isostatic residual geoid. These are for example the geoid low extending from the northwestern Pacific over North America into the central Atlantic and the low over India and Siberia, continuing to Antarctica.

A joint analysis of residual topography and residual and isostatic gravity has been performed to reveal and to discriminate the effects of upper-mantle density anomalies, mantle flows and deep density heterogeneities. Significant dynamical support associated with a low-density mantle is assumed in the North Atlantic, the eastern border of Eurasia and the northeast of Australia, while for the regions southeast of Australia and over western North America, the positive residual topography does not seem to be dynamically supported.

The isostatic residual geoid is evaluated by comparing it with model geoids calculated from different seismological models of the Earth's deep interior. The power spectra reveal similarities in their long-wave parts. In particular, the minimum at degree 4 of the isostatic residual geoid's power spectrum is believed to originate from deep-mantle inhomogeneities and discontinuities, which also have a low power at degree 4, as inferred from global seismological models. This agreement makes it clear that the isostatic residual geoid reflects the impact of deep-seated inhomogeneities on the external gravitational potential more accurately than the observed geoid.

NOTE

The global gravity and geoid models shown in the figures are available via ftp in digital format either as spherical harmonic coefficients or as grid values upon request to P. Schwintzer (e-mail: psch@gfz-potsdam.de).

ACKNOWLEDGMENTS

We would like to thank Dr W. D. Mooney for the very useful discussion and for providing the digital version of the CRUST 5.1 database. The authors are grateful to Dr V. M. Gordin for his assistance, comments and discussions. This work was supported by GeoForschungsZentrum Potsdam (GFZ) and in particular by Prof. Ch. Reigber, who enabled the Russian authors to work with GFZ during the course of this study. The colour plots were produced using the freely available plot software, Generic Mapping Tools (GMT 3.0) (Wessel & Smith 1995). We also thank the anonymous reviewers for comments which helped to improve the paper.

REFERENCES

Arfken, G., 1968. *Mathematical Methods for Physicists,* Academic Press, New York.

Artemjev, M.E. & Kaban, M.K., 1986. The free mantle surface—new possibilities to reveal subcrustal inhomogeneities from the structure of the Earth crust, *J. Geodyn.,* **5,** 25–44.

Artemjev, M.E. & Kaban, M.K., 1987. Isostasy and cross-spectral method of its study, *Phys. Solid Earth,* **23,** 935–945.

Artemjev, M.E. & Kaban, M.K., 1991. Isostatic processes and intracontinental orogenesis, *J. Geodyn.,* **13,** 77–86.

Artemjev, M.E. & Kaban, M.K., 1994. Density inhomogeneities, isostasy and flexural rigidity of the lithosphere in the Transcaspian region, *Tectonophysics,* **240,** 281–297.

Artemjev, M.E., Kaban, M.K., Kucherinenko, V.A., Demjanov, G.V. & Taranov, V.A., 1994. Subcrustal density inhomogeneities of the

northern Eurasia as derived from the gravity data and isostatic models of the lithosphere, *Tectonophysics,* **240,** 248–280.

Belousov, V.V., ed., 1987. *Karta rel'efa poverhnosti mantii Evrazii, Masstab 1 : 15 000 000* (The map of the mantle surface relief of Eurasia, scale 1 : 15 000 000), Izdanie Instituta Fiziki Zemli Akad. Nauk SSSR i Ministerstva Geologii Rossiyskoy Federatsii, Moskva (in Russian).

Cazenave, A., Dominh, K., Allegre, C.J. & Marsh, J.G., 1986. Global relationship between oceanic geoid and topography, *J. geophys. Res.,* **91,** B, 11 439–11 450.

Chapman, M.E. & Bodine, J.H., 1979. Considerations of the indirect e ect in the marine gravity modelling, *J. geophys. Res.,* **84,** B, 3889–3892.

Chase, C.G. & McNutt, M.K., 1982. The geoid: e ect of compensated topography and uncompensated oceanic trenches, *Geophys. Res. Lett.,* **9,** 29–32.

Dahlen, F.A., 1981. Isostasy and the ambient state of stress in the oceanic lithosphere, *J. geophys. Res.,* **86,** B, 7801–7807.

Davis, E.E. & Lister, C.R.B., 1974. Fundamentals of ridge crest topography, *Earth planet. Sci. Lett.,* **21,** 405–413.

Dorman, L.M. & Lewis, B.T.R., 1970. Experimental isostasy. 1. Theory of determination of the Earth's isostatic response to a concentrated load, *J. geophys. Res.,* **75,** B, 3357–3365.

Drewry, D.J., 1983. *Antarctica: Glaciological and Geophysical Folio,* Polar Res. Inst., Cambridge.

Dziewonski, A.M. & Anderson, D.L., 1981. Preliminary reference Earth model, *Phys. Earth planet. Inter.,* **25,** 297–356.

Forte, A.M., Peltier, W.R., Dziewonsky, A.M. & Woodward, R.L., 1993. Dynamic surface topography: a new interpretation based upon mantle flow models derived from seismic tomography, *Geophys. Res. Lett.,* **20,** 225–228.

Hager, B.H., 1983. Global isostatic geoid anomalies for plate and boundary layer models of the lithosphere, *Earth planet. Sci. Lett.,* **63,** 97–109.

Hager, B.H. & Clayton, R.W., 1989. Constraints on the structure of mantle convection using seismic observations, flow models, and the geoid, in *Mantle Convection: Plate Tectonics and Global Dynamics,* pp. 657–764, ed Peltier, W.R., Gordon & Breach, New York.

Haxby, W.F. & Turcotte, D.L., 1978. On isostatic geoid anomalies, *J. geophys. Res.,* **83,** B, 5473–5478.

Heiskanen, W. & Moritz, H., 1967. *Physical Geodesy,* W.H. Freeman, San Francisco.

Hurtig, E., Cermak, V., Haenel, R. & Zui, V., eds, 1992. *Geothermal Atlas of Europe,* 1st edn, Hermann Haack Verlagsgesellschaft, Gotha.

IAG, 1971. International Association of Geodesy: Geodetic Reference System 1967, *Bull. Géod.,* Publ. Spec. No. 3, Paris.

Jenkins, G.M. & Watts, D.G., 1968. *Spectral Analysis and its Applications,* Holden-Day, San Francisco.

Jordan, T.H., 1981. Continents as a chemical boundary layer, *Phil. Trans. R. Soc. Lond.,* A, **301,** 359–373.

Jordan, T.H., 1988. Structure and formation of the continental tectosphere, *J. Petrol.,* Special Lithosphere Issue, **29,** 11–37.

Kenyon, S.C. & Pavlis, N.K., 1996. The development of a global surface gravity data base to be used in the joint DMA/GSFC geopotential model, in *Global Gravity Field and its Temporal Variations,* pp. 82–91, eds Rapp, R.H., Cazenave, A.A. & Nerem, R.S., *IAG Symposia,* No. 116, Springer, Berlin.

Langseth, M.G., Jr., Le Pichon, X. & Ewing, M., 1966. Crustal structure of the mid-ocean ridges, 5. Heat flow through the Atlantic Ocean floor and convection currents, *J. geophys. Res.,* **71,** B, 5321–5355.

Lemoine, F.G., Pavlis, N.K., Kenyon, S.C., Rapp, R.H., Pavlis, E.C. & Chao, B.F., 1998. New high-resolution model developed for Earth's gravitational field, *EOS, Trans. Am. geophys. Un.,* **79,** 113–118.

Le Stun , Y. & Ricard, Y., 1995. Topography and geoid due to lithospheric mass anomalies, *Geophys. J. Int.,* **122,** 982–990.

Lister, G.R.B., 1982. Geoid anomalies over a cooling lithosphere: source for a third kernel of upper mantle thermal parameters and thus an inversion, *Geophys. J. R. astr. Soc.,* **68,** 219–240.

McKenzie, D.P, 1967. Some remarks on heat flow and gravity anomalies, *J. geophys. Res.,* **72,** B, 6261–6273.

Mooney, W.D. & Braile, L.W., 1989. The seismic structure of the continental crust and upper mantle of North America, in *The Geology of North America,* Vol. A, *Overview,* pp. 39–52, eds Bally, A.W. & Palmer, A.R., GSA, Boulder, CO.

Mooney, W.D., Laske, G. & Masters, T.G., 1998. CRUST 5.1: A global crustal model at $5^\circ \times 5^\circ$, *J. geophys. Res.,* **103,** B, 727–747.

Morelli, A. & Dziewonski, A.M., 1987. Topography of the core-mantle boundary and lateral homogeneity of the liquid core, *Nature,* **325,** 678–683.

Müller, R.D., Roest, W.R., Royer, J.-Y., Gahagan, L.M. & Sclater, J.G., 1993. *A Digital Age Map of the Ocean Floor,* Scripps Inst. of Oceanography, SIO Reference Series No. 93–30, University of California, San Diego.

Ockendon, J.R. & Turcotte, D.L., 1977. On the gravitational anomalies due to thin mass layers, *Geophys. J. R. astr. Soc.,* **48,** 479–492.

Parsons, B. & Sclater, J.G., 1977. An analysis of the variation of ocean floor with age, *J. geophys. Res.,* **82,** B, 803–827.

Pavlis, N.K. & Rapp, R.H., 1990. The development of an isostatic gravitational model to degree 360 and its use in global gravity modelling, *Geophys. J. Int.,* **100,** 369–378.

Rapp, R.H. & Yi, Y., 1991. *The October 1990 1 × 1 degree mean anomaly file including on analysis of gravity information from China,* Ohio State University, Dept Geod. Sci. & Surv., Internal Report, Columbus, OH.

Ricard, Y., Richard, M., Lithgow-Bertelloni, C. & Le Stun , Y., 1993. A geodynamic model of mantle density heterogeneity, *J. geophys. Res.,* **98,** B, 21 895–21 909.

Schwintzer, P. *et al.*, 1997. Long-wavelength global gravity field models: GRIM4-S4, GRIM4-C4, *J. Geod.,* **71,** 189–208.

Sclater, J.G. & Francheteau, J., 1970. The implications of terrestrial heat flow observations on current tectonic and geochemical models of the crust and upper mantle of the Earth, *Geophys. J. R. astr. Soc.,* **20,** 509–542.

Shearer, P.M., 1993. Global mapping of upper-mantle reflectors from long-period *SS* precursors, *Geophys. J. Int.,* **115,** 878–904.

Simons, M. & Hager, B.H., 1997. Localization of the gravity field and the signature of glacial rebound, *Nature,* **390,** 500–504.

Strakhov, V.N., Romaniuk, T.V. & Frolova, N.K., 1989. Method of direct gravity problem solution for modeling of global and regional gravity anomalies, in: *New Methods of Gravity and Magnetic Anomaly Interpretation,* pp. 118–235, ed. Strakhov, V.N., Inst. Phys. Earth, Moscow (in Russian).

Sünkel, H., 1986. Global topographic–isostatic models, in: *Lecture Notes in Earth Sciences,* No. 7, *Mathematical and Numerical Techniques in Physical Geodesy,* pp. 417–462, ed. Sünkel H., Springer, Berlin.

Tanimoto, T., 1990. Long-wavelength *S*-wave velocity structure throughout the mantle, *Geophys. J. Int.,* **100,** 327–336.

Turcotte, D.L. & Oxburgh, E.R., 1967. Finite amplitude convective cells and continental drift, *J. Fluid Mech.,* **28,** 29–42.

Vening Meinesz, F.A., 1946. The indirect isostatic or Bowie reduction and the equilibrium figure of the Earth, *Bull. Géod.,* **1,** 33–107.

Vidale, J.E. & Mooney, W.D., 1998. The Earth's topography: the influence of the crust and the upper mantle, *Geology,* submitted.

Wessel, P. & Smith, W.H.F., 1995. New version of the Generic Mapping Tools released, *EOS, Trans. Am. geophys. Un.,* **76,** 329.

White, R.S., McKenzie, D.P. & O'Nions, R.K., 1992. Oceanic crustal thickness from seismic measurements and rare Earth element inversions, *J. geophys. Res.,* **97,** B, 19 683–19 715.

Wieser, M., 1987. *Das globale digitale Höhenmodell TUG87,* Interner Bericht, Technische Univ. Graz.

APPENDIX A: METHOD OF EXPERIMENTAL ADMITTANCE DETERMINATION

Fourier transforms or spherical harmonic expansion is usually used to determine experimental admittances according to

eq. (12). In the case of a global analysis the spherical harmonic expansion of global topography and gravity provides a direct estimation of the experimental admittance coe cients, but for investigating non-global tectonic units neither Fourier transforms nor spherical harmonic expansion is appropriate when applied in a straightforward approach. It is necessary to introduce a special 'tectonic' function when using a spherical harmonic expansion for a restricted area. This function is equal to one over the area under investigation and to zero for the rest of the world. This leads inevitably to strong 'edge' e ects systematically degrading the resulting admittance coe cients. The same is true for Fourier transforms, where the area under investigation must be rectangular, and spherical e ects are neglected. To overcome these problems, the computation procedure was modified. Instead of a direct determination of cross- and power-spectra in eq. (12), the autocovariance $\gamma_{pp}(r_x, r_y)$ and cross-covariance $\gamma_{gp}(r_x, r_y)$ functions of the residual topography and gravity fields were initially computed (r_x, r_y are components of the correlation radius vector $\mathbf{r}$). Their Fourier transformations give the power- and cross-spectra (Jenkins & Watts 1968), but, as a 2-D transfer function (admittance) is not needed, the covariances are first averaged over discrete bands of $\mathbf{r}$, leaving a dependence only on its modulus $r = \sqrt{r_x^2 + r_y^2}$. Then, the averaged cross- and power-spectra, as defined in eq. (12), can be found using Hankel transformation of the averaged covariances (Arfken 1968):

$$\langle P(\mathbf{k})P^*(\mathbf{k})\rangle = \int_0^\infty \langle\gamma_{pp}(r_x, r_y)\rangle r J_0(kr)dr\,,$$
$$\langle G(\mathbf{k})P^*(\mathbf{k})\rangle = \int_0^\infty \langle\gamma_{gp}(r_x, r_y)\rangle r J_0(kr)dr\,, \tag{A1}$$

where J_0 is the zero-order Bessel function and angle brackets indicate averaging over the discrete bands of $\mathbf{r}$ and $\mathbf{k}$, respectively. These values may be directly used in eq. (12) to estimate the experimental admittance coe cients, which then depend only on the modulus $\sqrt{k_x^2 + k_y^2}$ of the wave vector $\mathbf{k}$.

This technique of admittance calculation has some advantages compared to the traditional technique:

(1) cross- and autocovariances are normally centre-weighted functions and it is much easier to reduce edge e ects during their transformation into cross- and power-spectra than while making Fourier transformations or spherical harmonic expansions of the initial gravity and topography;

(2) while computing cross- and autocovariances, it is possible to determine the distance between two points directly on the Earth's sphere, thereby avoiding distortions when projecting any piece of the Earth's sphere before making a Fourier transformation;

(3) it is possible to determine cross- and autocovariance functions of the gravity field and topography for an area of any shape (theoretically even for disconnected areas).

It is known from experience that possible systematic distortions may significantly a ect the experimental admittance function (Artemjev & Kaban 1987, 1991). The main factor which causes such distortions is the influence of structures which are placed outside the analysed area but significantly contribute to the anomalous gravity field within the area. This is particularly important in the case of global studies. If one uses an expression such as eq. (11) for a direct determination of the e ective compensation depth by fitting Z to the experimental admittance function and is not bothered about possible systematic distortions, the resulting depth may be in error by a factor of 2 or more.

A simple method proposed by Artemjev & Kaban (1991) was used to ensure the reliability of the admittance function determination. Three synthetic lithosphere gravity fields resulting from the residual topography field and opposite mass anomalies at adopted compensation levels of 25, 50 and 75 km depth were calculated by a 3-D forward computation for the equal-angular grid over the whole Earth. Then, for each area under investigation, the admittance functions based on the computed synthetic gravity fields and the residual topography were calculated in the same way as the experimental admittances. It is reasonable to assume that possible systematic distortions of the experimental admittances will a ect the synthetic admittances found for the three compensation levels in the same way. Therefore, for each particular area under study, the values of the empirical admittance function, calculated from the observed data according to eq. (12), were interpolated by a least-squares adjustment between the synthetic admittance curves to find the e ective level of compensation.